LBL-9234

First Results from the Berkeley-Fermilab-Princeton Multimuon Spectrometer*

Mark Strovink

Department of Physics and Lawrence Berkeley Laboratory,
University of California, Berkeley, California 94720

Invited Paper Presented at the
Seminar on Probing Hadrons with Leptons
"Ettore Majorana" Centre for Scientific Culture
Erice, Trapani, Sicily
March 13-21, 1979

Muon interactions in a magnetized-steel calorimeter have produced 1000±80 muons from $J/\psi(3100)$ decay, and 3 final states containing >3 energetic muons. Use of proportional and drift chambers fully sensitive in the forward direction has resulted in uniform high acceptance for these processes, with 9% mass resolution. The ψ photoproduction cross section continues to rise above 30 GeV, at a rate smaller than that predicted by a QCD calculation. Its Q^2-dependence fits $(1+Q^2/M^2)^{-2}$ with M=2.7±0.5 GeV.

* Research performed by A.R. Clark, K.J. Johnson, L.T. Kerth, S.C. Loken, T.W. Markiewicz, P.D. Meyers, W.H. Smith, M. Strovink, and W.A. Wenzel (Berkeley); R.P. Johnson, C. Moore, M. Mugge, and R.E. Shafer (Fermilab); G.D. Gollin, F.C. Shoemaker, and P. Surko (Princeton).

FIRST RESULTS FROM THE BERKELEY-FERMILAB-PRINCETON MULTIMUON SPECTROMETER*

Mark Strovink

Department of Physics and Lawrence Berkeley Laboratory
University of California, Berkeley, California 94720

INTRODUCTION

For the purpose of performing a highly sensitive study of muon-induced final states containing 1, 2, 3, 4, or 5 muons, data have collected with a new spectrometer in the Fermilab muon beam. Examples of rare multimuon events and first results on $J/\psi(3100)$ production by muons are presented in this report.

In early 1973 we proposed[1] to study multimuon final states at Fermilab using a spectrometer with target thickness and acceptance far exceeding that envisaged in other muon experiments. Of interest were a search for the heavy neutral muon (M^0) predicted by various theories of weak interactions with spontaneously broken gauge symmetry (Fig. 1(a)), and the study of deep-inelastic virtual Compton scattering (Fig. 1(b)). By 1975, observations[2] of the $J/\psi(3100)$ had led us to expect[3] hidden and open charm to be manifested in a variety of muon-produced multimuon final states -- ψ production with $\mu^+\mu^-$ decay (Fig. 1(c)), and charmed hadron pair production with one or two semileptonic decays into a muon (Fig. 1(d)). The discovery[4] of scale-noninvariance in lepton-nucleon scattering in the Fermilab muon beam emphasized the need to extend measurements of nucleon structure functions to higher Q^2.

---

* Research performed by A.R. Clark, K.J. Johnson, L.T. Kerth, S.C. Loken, T.W. Markiewicz, P.D. Meyers, W.H. Smith, M. Strovink, and W.A. Wenzel (Berkeley); R.P. Johnson, C. Moore, M. Mugge, and R.E. Shafer (Fermilab); G.D. Gollin, F.C. Shoemaker, and P. Surko (Princeton).

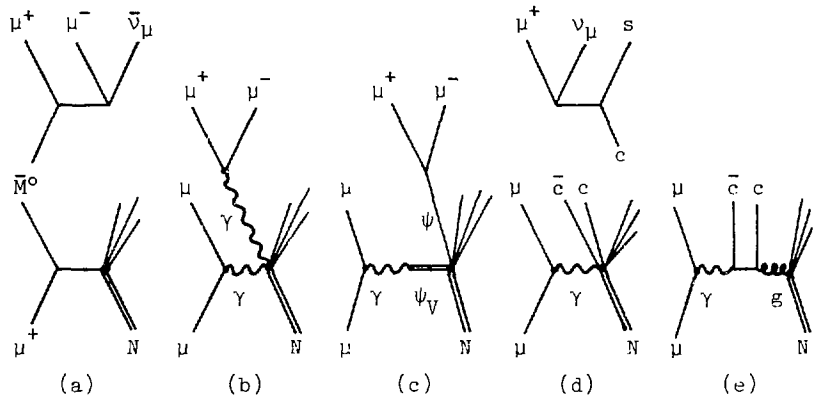

Fig. 1. Feynman diagrams.(a) $\bar{M}^0$ production and decay; (b) virtual Compton scattering; (c) ψ production; (d) $c\bar{c}$ production and decay; (e) "photon-gluon-fusion" (additional gluon exchange is necessary to conserve color).

THE MULTIMUON SPECTROMETER

In the Fermilab muon beam the desired luminosity ($\gtrsim 10^6$ nb^{-1} per experiment) could be achieved with a massive target ($\sim$5 kg/cm^2). High acceptance over the full target length made necessary a spectrometer magnet integral with the target. Its steel plates were desirable also as hadron absorbers for calorimetry and muon identification. The earliest computer simulations of multimuon final states underscored the necessity for full acceptance in the forward direction, with no blind "beam hole". Inability to determine the momentum of muons scattered or produced near 0° would remove vital analysis constraints; inability to find all the final-state muons would alter drastically the interpretation of many events. A dipole field configuration, requiring only one pair of coils for the full magnet, was most compatible with high forward acceptance. Proportional and drift chambers could withstand the full beam flux at Fermilab (typically 2×10^6 muons per 1-sec spill) without deadening in the beam area. With this design, the spectrometer optimized and extended the utility of the existing beam.

Construction of the apparatus depicted in Fig. 2 was completed in 1977. It consists of 18 25-ton modules each containing 5 10-cm-thick steel plates, 5 calorimeter scintillators (omitted in modules 16-18), and a pair of proportional (PC) and drift chambers (DC). Banks of 12 trigger scintillators (S_1-S_{12}) are located in even modules 4-18. The fiducial volume, 1.8 x 1 m^2 in area, extends 16 *m* in the beam direction. Within the central 1.4 x 1 m^2 area of each magnet plate, the 19.7 kgauss field is uniform to 3% and mapped to

0.2%. Located upstream of module 1 are one additional PC and DC, 63 beam scintillators, 8 beam PC's, and 94 scintillators sensitive to accidental beam and halo muons.

Figure 3(a) is an exploded view of the detectors in a gap between modules. The 2 -cm drift chamber cell and specially designed readout electronics make possible a system efficiency exceeding 98% during high-rate ($\lesssim 10^7$ Hz) conditions.[5] Twofold DC ambiguities are resolved by the PC anode wires, spaced at Δx = 3 mm. Coordinates at 30° (u) and 90° (y) to the bend direction (x) are registered in the proportional chambers by means of 5-mm wide cathode strips. Each strip is connected to one input of a differential amplifier in the network shown in Fig. 3(b). Although spread over many cathode strips, the induced charge produces a count only in the one or two electronics channels closest to the peak, even when the pulse height far exceeds threshold. Through a specially stabilized amplifier, each calorimeter scintillator feeds two ADC's, which together operate over a range of 0.03 to 1500 equivalent minimum-ionizing particles. The resolution on hadron energy E_{had}, calibrated using inelastic muon scattering, is $1.5E_{had}^{\frac{1}{2}}$ (GeV).

The spectrometer was triggered in parallel by ≥ 1, ≥ 2, or ≥ 3 muons in the final state. The required signatures in the scin-

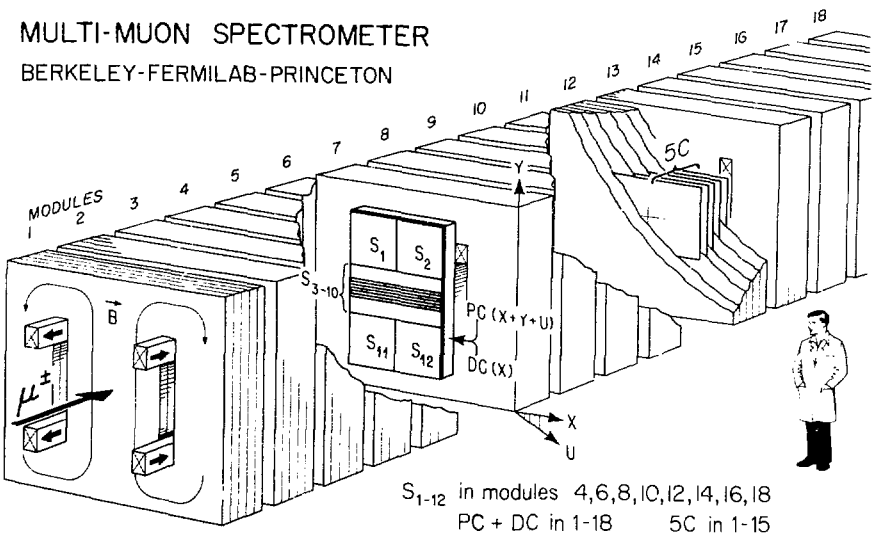

Fig. 2. Schematic view of apparatus. S_1 - S_{12} are trigger scintillators. PC and DC are proportional and drift chambers. The scintillators labelled 5C perform hadron calorimetry.

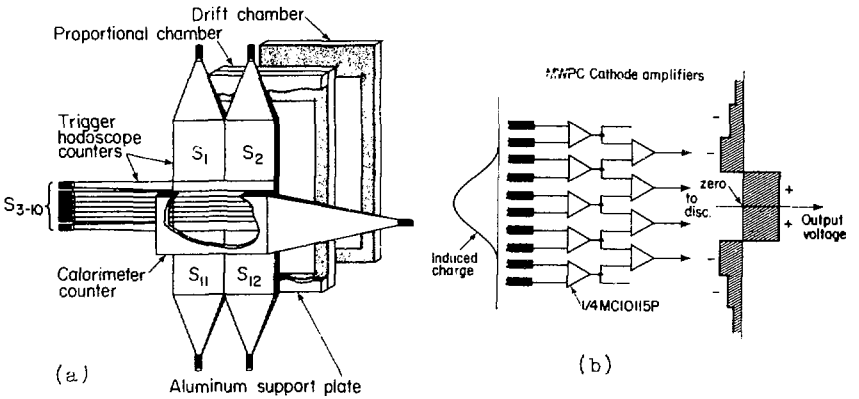

Fig. 3. Apparatus detail. (a) exploded view of detectors within a typical gap between magnet modules; (b) network of differential amplifiers sensing center of charge distribution induced on proportional-chamber cathode strips.

tillator hodoscopes and calorimeter counters are listed in Table 1. The multimuon triggers could not be vetoed by hodoscope and calorimeter information; the $\geq 1\mu$ and $\geq 3\mu$ triggers were affected in no way by the calorimeter signals. Under some conditions, when more than one count was required from a scintillator hodoscope, two of the contributing hodoscope elements were required not to be adjacent. During the run the instantaneous beam intensity varied from 0.03 to 0.11 muon per RF bucket. Each bucket was separated from the

Table 1. Trigger requirements for $\geq 1\mu$, $\geq 2\mu$, and $\geq 3\mu$ final states.

Final state	Requirements in each of 3 consecutive trigger banks	Requirement in calorimeter
$\geq 1\mu$	$A \cdot \bar{B}^a$	no requirement
$\geq 2\mu$	≥ 2 in A or B	≥ 20 GeV deposited ≥ 2 modules upstream
$\geq 3\mu$	≥ 3 in A or B	no requirement

[a] "B" refers to S_3-S_{10} in Figs. 2 and 3(a); "A" refers to S_1, S_2, S_{11}, and S_{12}.

next by 19 nsec. The trigger was vetoed by halo muons in the same RF bucket, or beam muons in the same or adjacent buckets. The deadtime thereby induced ranged up to ∿50%. As many as ∿60 events/1-sec spill were recorded on a PDP-15 computer with read-in deadtime ≲15%.

EVENT RECONSTRUCTION AND SIMULATION

Beam muons were momentum-analyzed by systems of proportional chambers and scintillator hodoscopes interspersed between magnets producing two separate beam deflections. Pulse heights from calorimeter counters within the spectrometer provided a tentative longitudinal vertex position, using algorithms which depended on the type of trigger. The beam track then was traced forward to this vertex using the PC and DC hits. Outgoing tracks were recognized initially at their downstream end. Hits were added extending the tracks upstream to the vertex, making adequate allowance for Coulomb scattering and momentum uncertainty. In order not to interfere with rejection of halo tracks or later use of outgoing tracks to pinpoint the vertex, the transverse vertex position was not allowed to influence this upstream projection. At least 4 PC hits in two views and 3 hits in the third view were required for each accepted track. The small electromagnetic showers found along high-energy muon tracks in iron, due mainly to direct production of electron pairs, contributed extra hits in the wire chambers which were not completely rejected at this stage. After the full track was identified, it was possible to apply a complex momentum-fitting algorithm capable of solving for the Coulomb-scattering angle in each magnet module, yielding a rigorous χ^2 for the track. By iteration, this algorithm identified and suppressed the false extra hits.

The beam and secondary tracks next were examined for consistency with a common vertex. The vertex position was moved by iteration in 3 dimensions to minimize the overall χ^2 while including all associated tracks. This iteration provided an opportunity to finalize the inventory of hits on the tracks. After the vertex was fixed, the coordinates and momentum of each track were redetermined subject to the condition that it intersect the vertex point.

For analysis of 1μ final states (inelastic scattering) and some 3μ final states (ψ production), the events were subjected to a 1-constraint fit demanding equality between the beam energy at the interaction point and the sum of muon and hadron shower energies in the final state. Using error matrices produced by the fits to individual tracks, the constraint perturbed all components of each track momentum. The resulting momentum resolution is 7%-12% (typically 8%) per track. At the ψ mass, the dimuon mass resolution is 9%. The uncertainty in Q^2 typically is 10%, but is bounded below by ∿0.15 $(GeV/c)^2$ because of track angle uncertainty. The strong features of the analysis described above -- rigorous criteria for accepting hits on tracks, precise track definition close to the

common vertex, and energy-conserving 1C fit -- establish our confidence in its results.

The acceptance and resolution of the spectrometer were modeled by a complete Monte Carlo simulation. Coordinates of randomly sampled beam muons were used to represent the beam. Simulated muons underwent single and multiple Coulomb scattering, bremsstrahlung, and other energy-loss straggling in the steel magnet plates. Their trajectories were deflected in each plate by the precisely mapped magnetic field. Simulated interactions occurred between muons and nucleons in non-degenerate Fermi motion, or coherently between muons and Fe nuclei. At low momentum transfer the effects of nuclear scattering were taken into account. Coherent and elastic processes were attenuated by the appropriate form-factors even for forward scattering (at $|t|_{min}$). Detector resolutions and efficiencies were included throughout. Monte Carlo events were output in the same magnetic tape format as raw data, and were reconstructed, momentum-fit and histogrammed by the same programs.

COPIOUS AND RARE EVENTS

Data were accumulated during the first half of 1978 using $\sim 4 \times 10^{11}$ (gated) 213-GeV muons, of which $\sim 90\%$ were μ^+. Approximately 5×10^9 100-GeV μ^+ also were used. The extent of the data is shown in Table 2. Events with 2 or 3 muons in the final state, or with $Q^2 > 50$ $(GeV/c)^2$, are not rare in this experiment -- at least 10^5 of each category are on tape. "Rare" events thereby are redefined as those having ≥ 4 muons or 2 missing leptons in the final state.

Identification of rare events begins in the programs which reconstruct muon tracks and fit their momenta. Events satisfying normal analysis criteria which possess unusual characteristics are saved on microfilm containing tabulated data and computer-generated

Table 2. Extent of data.

Final state	Cuts	Total on tape
1μ	$Q^2>10$	10^6
	$Q^2>50$	10^5
	$Q^2>100$	10^4
2μ	$E_{slow} \gtrsim 10$ GeV	2×10^5
3μ	$E_{slow} \gtrsim 10$ GeV	2×10^5
	ψ (background subtracted)	10^5

track pictures. A double scan by physicists of the microfilm identifies a small sample of candidates for which are generated $\sim$1 m^2 pictures containing all raw wire chamber hits, resolved to better than 1 mm in real transverse coordinates. With the high-resolution pictures, raw chamber hits are reconstructed by hand into tracks and the vertex position determined. The track reconstruction program then is forced to fit the event using the hand-selected information. To be accepted as a rare event, the result of this hand-forced fit is required to differ in no significant respect from that of the original reconstruction. Close inspection of each high-resolution picture insures that additional tracks crossing as few as 3 chambers have not been missed, and that distinct tracks separated along their full length by as little as 5 mm have not been combined. A particular concern, that two interactions not mistakenly be superimposed, is satisfied by four precautions: (1) The trigger demands only one beam track within a 57-nsec window centered on the event. (2) All tracks are required to emanate from a tightly defined common vertex. (3) All tracks are required to register in the appropriate fine-grained hodoscope scintillators, sensitive within a $\pm$10 nsec window. (4) Adjacent drift and proportional chamber hits are required to register at a level rejecting tracks out of time by more than $\sim$50 nsec. The accepted tracks satisfy a tight χ^2 cut separately in both orthogonal views. At least three hits in the third view unambiguously link the two projections. Each accepted track, passing smoothly through >12 absorption lengths of steel, can be interpreted only as a muon. The sign of each muon's charge is at least 8 standard deviations from the reversed value.

Table 3 presents the properties of four rare events found in an initial scan of 20% of the data. They consist of one 3μ event with two missing μ^- or ν_μ, one 4μ event with large pair masses, and two 5μ events. The efficiency of the initial scan exceeded 50%, with the possible exception of the 3μ event type. Although model-dependent, the detection efficiencies for these events may be estimated to lie typically in the 10%-20% range. Each event therefore represents a cross-section of order 3×10^{-38} cm^2/nucleon.

3μ Event (Two Missing Leptons)

Four events of this type have been produced by neutrino interactions in the CDHS apparatus[6], at a rate consistent with π/K decay contamination of dimuon events. The small pair masses and transverse momenta in event 851-5726 favor such an interpretation. The size of the corresponding dimuon sample places a bound on the probability of π/K decay into a detectable muon ($\geq$10 GeV). This probability is less than 10^{-4} per hadron shower in the apparatus.

5μ Events

No 5-muon final state (or 4-muon final state with other than

μ or ν_μ incident) has been observed in any previous experiment. It is natural to try to interpret events 1208-3386 and 851-11418 as QED phenomena ("muon pentads"). Their negligible hadronic and missing energies support such an interpretation. Event 1208-3386 possesses values of Q^2, pair masses, and daughter transverse momenta typical of muon tridents, which are more abundant by a factor consistent with α^{-2}. However, event 851-11418 has kinematic properties which are puzzling. To explore these properties, all lowest-order QED diagrams have been examined. One diagram has been found to minimize the product of the denominators in the lepton and photon propagators. It is a Bethe-Heitler-like graph with the incident muon scattered into track 2 and coupled to track 5, and the target coupled to track 3. Tracks 4 and 6 form a pair radiated by track 5. The unseen $p_\perp$ is 1.8±0.4; for the above choice of scattered muon, Q^2 is 3.5±0.6, and the daughter (unscattered) muons have a combined mass M_{3456}=3.5±0.3. Of the muon tridents observed in the same data

Table 3. Rare Events.

Event	Scattered Muon	Energies (GeV)	Masses (GeV/c^2)	Unseen $p_\perp$ to $\gamma\gamma$ (GeV/c)
851-5726	2	E_3= 19± 2	M_{34}=0.5±0.1	0.3±0.1
$\mu^- \to \mu^- \mu^+ \mu^+$	Q^2=0.1±0.1	E_4= 11± 2		
1 2 3 4	ν =160±6	E_{had}=103±15		
		E_{miss}= 27±17		
1191-5809	2	E_3= 26± 3	M_{34}=3.0±0.3	2.0±0.2
$\mu^+ \to \mu^+ \mu^+ \mu^- \mu^-$	Q^2=0.3±0.2	E_4= 18± 2	M_{35}=3.2±0.3	
1 2 3 4 5	ν =158±7	E_5= 25± 4	M_{345}=4.6±0.3	
		E_{had}> 57±11		
		E_{miss}< 31±14		
1208-3386	2	E_3= 50± 5	M_{35}=1.3±0.2	0.1±0.3
$\mu^+ \to \mu^+ \mu^- \mu^- \mu^+ \mu^+$	Q^2=0.2±0.2	E_4= 27± 3	M_{36}=0.3±0.1	
1 2 3 4 5 6	ν =149±9	E_5= 61± 6	M_{45}=0.4±0.1	
		E_6= 10± 2	M_{46}=0.5±0.1	
		E_{had}= 6± 3	M_{3456}=2.0±0.2	
		E_{miss}= -4±13		
851-11418	Q^2=3.5±0.6	E_3= 13± 2	M_{34}=2.3±0.2	1.8±0.4
$\mu^- \to \mu^- \mu^- \mu^+ \mu^+ \mu^-$	ν = 61±12	E_4= 19± 2	M_{35}=2.0±0.2	
1 2 3 4 5 6		E_5= 15± 2	M_{46}=0.5±0.1	
		E_6= 10± 2	M_{56}=0.3±0.1	
		E_{had}= 5± 3	M_{3456}=3.5±0.3	
		E_{miss}= -1±13		

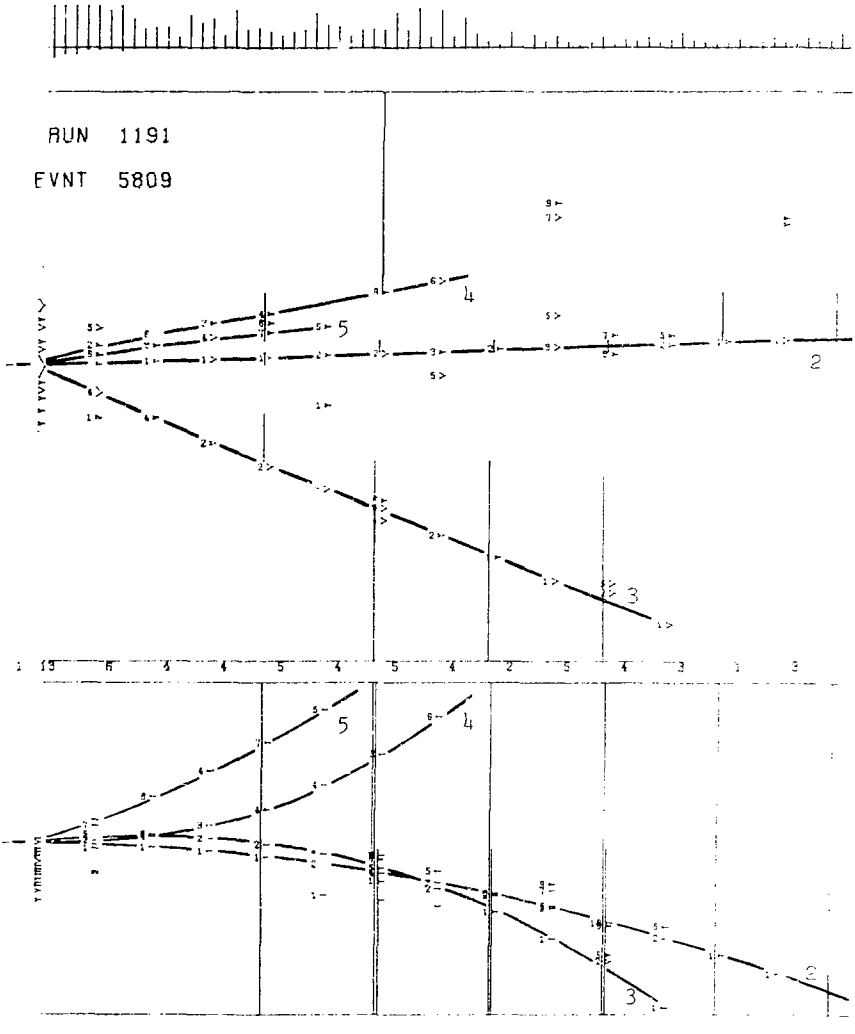

Fig. 4. Computer-generated picture of proportional-chamber hits in event 1191-5809. Top frame: elevation view; bottom frame: plan view. Short vertical lines at the top are calorimeter counter pulse heights. Long vertical lines are projections of trigger counters which were tagged. Heavy broken lines are tracings of the computer-reconstructed trajectories. Large (typed) numbers identify each track.

set, fewer than 200 have $Q^2>2.5$ and combined daughter muon mass >2.8; fewer than 20% of these have unseen $p_\perp$ >1.4 . A parent sample of that size would not be expected to yield one event with an additional energetic muon pair. The event requires a more plausible explanation.

High-Mass 4μ Event

One neutrino-induced four-lepton final state has been observed by each of three groups: CDHS[7], BFHWW[8], and HPWFOR[9]. The respective authors expect ∿1/5 of an event as background in the CDHS and HPWFOR samples, and $\sim 10^{-3}$ events in the BFHWW sample. The muon-induced 4μ event 1191-5809 is pictured in Fig. 4. Its kinematics are summarized in Table 3 and compared with those of the neutrino-induced events in Table 4. The muon-induced event is qualitatively different from the others. The softest lepton has at least 4x the energy and the lightest $\mu^+\mu^-$ daughter pair has at least 4x the mass of any neutrino-induced counterpart.

A relatively model-independent limit can be placed on this event's most obvious potential background -- single muon production due to any process, in *random* association with $\mu^+\mu^-$ pair production due to any process within the same diagram. Choosing the leading secondary (track 2) as the scattered muon produces the smallest Q^2 and determines the virtual photon direction, represented by the central axis of Fig. 5. The $\mu^+\mu^-$ pair is interpreted as that formed by tracks 3 and 4, because it is no more massive than that formed by tracks 3 and 5, but has only half the transverse momentum. Let

N_0=calculated no. of μ scatters with $y>1/2$ corresponding to the sensitivity of this data set.

Table 4. Comparison of event 1191-5809 to published neutrino-induced 4-lepton events.

Group	Final state leptons	Smallest lepton energy (GeV)	Smallest $\mu^+\mu^-$ or e^+e^- pair mass $(GeV/c)^2$
CDHS	$\mu^+\mu^-\mu^+\mu^-$	4.5	0.4
BFHWW	$\mu^+e^-e^+e^-$	0.9	0.8
HPWFOR	$\mu^-\mu^+\mu^+\mu^?$	3.0	0.5
This experiment	$\mu^+\mu^+\mu^-\mu^-$	18.3	3.0

N_1=observed no. of 2μ final states in which $y>1/2$ and the nonleading μ has $E>15$ and $p_\perp>1.7$ (Fig. 5).
N_2=observed no. of 3μ final states with $E_{pair}>30$, $(\nu-E_{pair}) > 100$ GeV, and $M_{pair}>2.75$.

The number N_B of background events is then

$$N_B < \varepsilon_B N_1 N_2/(\varepsilon_1 \varepsilon_2 N_0),$$

where the ε's are detection efficiencies. Using $\varepsilon_B/\varepsilon_1\varepsilon_2<10$, $N_1<200$, $N_2<13$, and $N_0=3.7\times10^7$, one obtains $N_B<7\times10^{-4}$.

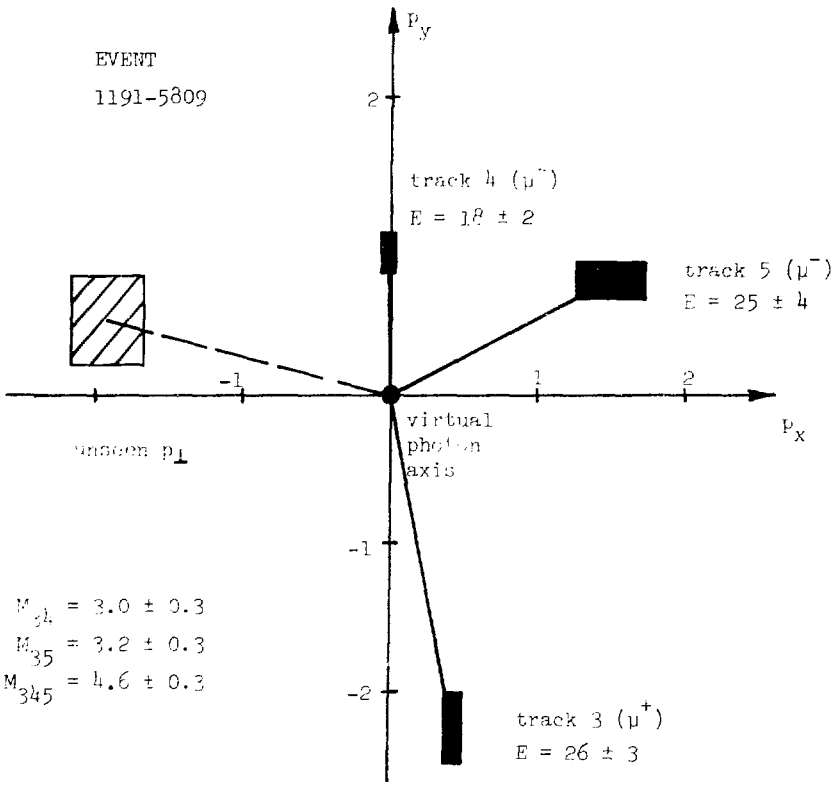

Fig. 5. Momenta transverse to the direction of the virtual photon in event 1191-5809. Dark boxes: secondary muons other than the scattered (spectator) muon. Hatched box: unseen transverse momentum carried off by neutrinos and/or hadrons. Box sizes indicate measurement errors.

Table 3 and Fig. 5 constrain kinematically the origin of this event. Rigorously, the parent system for the 3 daughter muons has a mass between 4.3 and 17.6 GeV (limits include one standard deviation in measuring error). If emitted at 90° in a frame travelling in the virtual photon direction, tracks 3, 4, and 5 require that frame to have γ=11.3, 19.1, and 14.9, for an average of 15.1. If this frame is the rest frame of a parent system carrying all of the virtual photon energy, the parent mass is 158/15.1=10.5 GeV. If the daughter muons are descendants of a heavy quark pair $Q\bar{Q}$ produced in the virtual photon direction, $M_Q > 4$ GeV. However, such cascades should produce a larger number of events not containing the analog of track 3. Both M_{34} and M_{35} are consistent with the ψ mass. If this ψ was produced by Drell-Yan fusion of charmed quarks, the third muon is most likely a descendant of the unfused member of the projectile charmed quark pair. This intepretation requires the charmed quarks to possess considerable transverse momentum. In any case, charmed-quark fusion is constrained by these data to account for no more than $\sim 10^{-2}$ of ψ photoproduction.

ONE-MUON AND TWO-MUON FINAL STATES -- ANALYSIS STATUS

The extent of data with one and two muons in the final state has been mentioned in Table 2. The acceptance for muon scattering is shown in Fig. 6. Four years have elapsed since the original observation of scale-noninvariance[4] in muon scattering. Systematic errors in the current analysis are steadily decreasing toward a level appropriate to new results in this mature field.

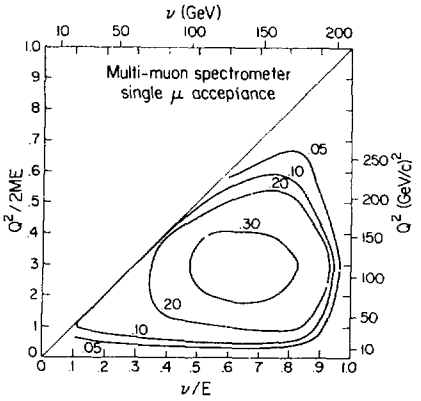

Fig. 6. Calculated detection efficiency vs. Q^2 and ν for inelastic muon scattering. An average over the full target length is shown. If the target is restricted to the few modules furthest upstream, the low-Q^2 acceptance is much more uniform.

The signatures for $\bar{M}^0$ production and decay in 2μ final states (Fig. 1(a)) are sufficiently unique that useful signal levels/limits can be determined even in the presence of copious background from charm production (Fig. 1(d)) and other sources. Such limits will be reported on the basis of a larger sample than has been analyzed at present. With the hadron calorimeter calibrated using inelastic scattering, substantial average missing energy is observed in the 2μ sample (Fig. 7(a)). Two-muon final states associated with backgrounds to charm production -- π/K decay, and $\mu^+\mu^-$ pair production with one muon undetected -- also are expected also to exhibit missing energy. Fig. 7(b) shows the missing energy associated with 3μ final states produced by highly inelastic muon interactions. When the $\mu^+\mu^-$ pair mass lies between the ψ region and the small values expected[10] from Bethe-Heitler and bremmstrahlung processes, the missing energy takes on a modest average value. In the 3μ channel, non-negligible backgrounds to pair-production of heavy quarks are expected to conserve visible energy. In comparison to the 2μ value, the average value of the 3μ missing energy suggests the presence of significant visible-energy-conserving background even in the intermediate-mass sample. Therefore it is clear that inelastic 3μ final states cannot naively be interpreted as arising

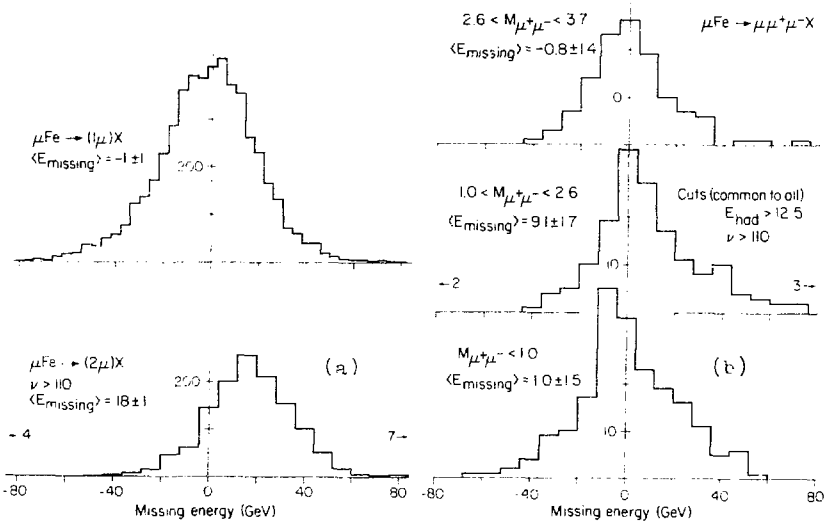

Fig. 7. Difference between beam energy and the sum of secondary muon and hadron shower energies at the vertex. (a) 1μ (top) and 2μ final states; (b) 3μ final states in three regions of $\mu^+\mu^-$ pair mass. The 1μ result is used to calibrate the calorimeter; the 2μ and 3μ results are sensitive to the indicated ν cut.

largely from charmed quark production and decay. When properly corrected for backgrounds, the same $c\bar{c}$ production cross-section should be measurable in final states containing three muons, opposite-sign muon pairs, and same-sign pairs.

J/ψ(3100) PRODUCTION BY MUONS

Previous experiments at Fermilab[11,12], SLAC[13], and Cornell[14] have measured ψ photoproduction. No previous experiment has detected ψ production by spacelike photons. Reported here are 1000±80 $\mu^+\mu^-$ pairs from ψ decay (Fig. 1(c)), drawn from 16834 muon interactions producing 3 fully-reconstructed muon tracks in the final state. These represent 12% of the data on tape.

Figure 8(a) displays the spectrum of $\mu^+\mu^-$ pair masses before and after continuum subtraction. The smoothness of the continuum emphasizes the uniformity of acceptance in the ψ mass region. Only one choice per event of $\mu^+\mu^-$ pairing is plotted. The unpaired (scattered) muon is taken to be the more energetic, if the candidates differ in energy by more than a factor of 2. Otherwise, it

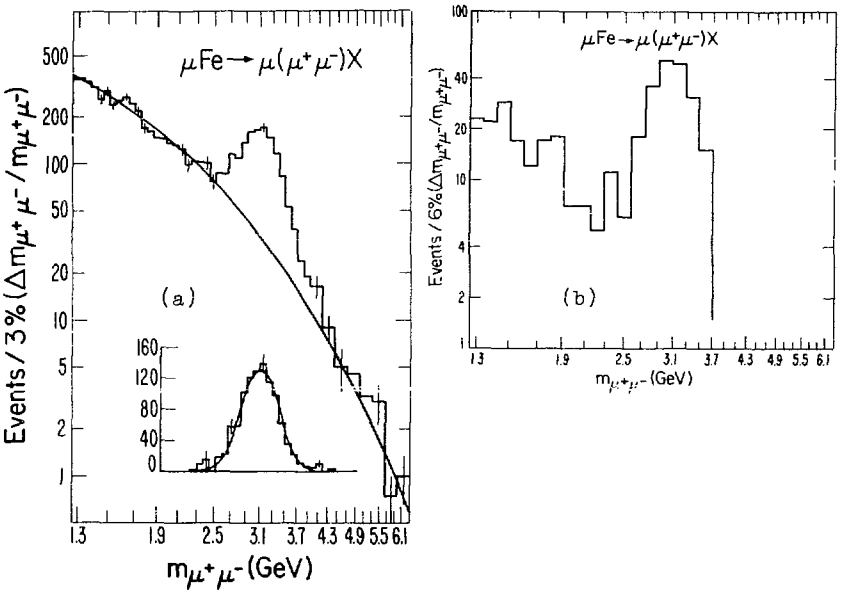

Fig. 8. Invariant mass spectrum of muoproduced $\mu^+\mu^-$. (a) All data, before and after subtraction of the continuum (representative fit is shown). The Gaussian curve is centered at 3.1 GeV with a 9% rms width. (b) Data with $(12\pm5) < E_{had} < (36\pm9)$.

is taken to be the candidate making the smallest angle relative to the beam direction. The effects of this and many alternate pairing algorithms have been studied extensively. Used on Monte Carlo events, this algorithm retains 92% of the ψ's in the mass peak and distributes the rest smoothly between 0.7 and 6 GeV. There is little tendency for mispaired events to dominate particular kinematic regions, such as high mass, Q^2, or ν. The same is not true for a number of other algorithms with similar overall probability of success in identifying the correct pair. Under less favorable experimental conditions, inability to reconstruct all 3 final state muons in effect can impose a pairing choice which is far from optimum. It is seen in Fig. 8(a) that the centroid of the ψ peak is consistent with 3.1 GeV, and its width with 9% rms. The latter is the average resolution calculated from first principles for each event, taking detector resolution and Coulomb scattering into account. It is also the width of the mass peak for Monte Carlo events. The effects on this mass spectrum of a $\psi' \to \mu^+\mu^-$ component at $\sim$5% of the ψ rate occur at the same subtle level introduced by possible variations in resolution shape, energy calibration, and continuum parameterization. A more promising method for studying the ψ' utilizes its cascade to hadrons + $\psi \to \mu^+\mu^-$. The ratio of hadron energy (detected in the calorimeter) to ψ energy is expected to peak at $\sim$0.2. Figure 8(b) shows the enhancement in the ψ peak relative to continuum when a moderate energy deposit in the calorimeter is required.

The data were absolutely normalized using optimum experimental conditions -- low beam intensity and an interaction region (first 8 magnet modules) allowing very long tracks downstream*. The effects of acceptance were removed by a Monte Carlo parameterization (described below) fitting all characteristics of the ψ sample. Allowing for the 7% $\psi \to \mu^+\mu^-$ branching ratio, the total cross-section is

$$\sigma/\text{nucleon}\ (\mu\ \text{Fe} \to \mu\psi X) = 0.76 \pm 0.22\ \text{nb}.$$

Monte Carlo corrections for nuclear coherence, shadowing, and $|t|_{min}$ effects yield

$$\sigma(\mu N \to \mu\psi X) = 0.67 \pm 0.20\ \text{nb}.$$

Essentially all the error is due to normalization uncertainty. A calculation[10] using the "photon-gluon-fusion" diagram (Fig. 1(e)) has yielded a cross-section consistent with this result.

In order to reproduce the experimental ratio of coherent to incoherent ψ production from Fe nuclei and to parameterize $|t|_{min}$ effects, the Monte Carlo simulation assumes the t-dependence of the

*If normalized using the full data sample, the cross-sections are reduced by less than one standard deviation.

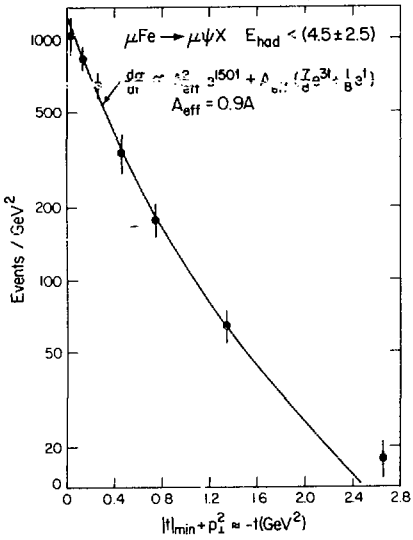

Fig. 9. Comparison of experimental t distribution to a Monte Carlo calculation (solid line) using the indicated parameterization of $d\sigma/dt$. The (unresolved) coherent component steepens the observed slope below $|t| \approx 0.5$.

cross section to be

$$d\sigma/dt\ (\gamma\ Fe \to \psi X) = G(t)\ d\sigma/dt\ (\gamma N \to \psi N)(t=0)$$
$$G(t) = A_e^2 \exp(\alpha t) + A_e[(1-\varepsilon\delta)\exp(\beta t) + \varepsilon\delta\exp(\delta t)]. \quad (1)$$

The t resolution of the spectrometer is such that a δ-function at t=0 is smeared into $\sim\exp(5t)$. Therefore, data from other photon-nucleus experiments[15], mainly at lower energies, are averaged to set the coherent slope α to 150 $(GeV/c)^{-2}$. The shadowing factor A_e is taken to be 0.9 x (A=55.85) based on electron-nucleus scattering data[16] at similar average Q^2. We have used β=3 $(GeV/c)^{-2}$, δ = 1 $(GeV/c)^{-2}$, and ε=1/8. These choices are consistent with high-energy ψ photoproduction data[11] and with the experimental t distribution, as shown in Fig. 9. In this and in Fig. 10, each data point is the result of a continuum subtraction like that in Fig. 8(a); the errors include uncertainties due to variation in the form and in the parameters used to fit the continuum. We have investigated the effects of varying α, A_e, β, δ, and ε over a range allowed by these data and (in the case of α and A_e) by other measurements. The effects on the shape of the Q^2 distribution are negligible. The effects on the E_γ distribution are summarized in Table 5. Variation of any one parameter "tilts" the distribution by less than $\sim$5%.

Table 5. Percent reduction in $d\sigma/dt(t=0)$ for ψ production by virtual photons, induced by variations in nuclear and nucleon parameters α $(GeV/c)^{-2}$, A_e, ε, β $(GeV/c)^{-2}$, and δ $(GeV/c)^{-2}$.

Parameter	α	A_e	ε	β	δ
Best value	150	50.27	1/8	3	1
Varied value	135	55.85	1/5	2.5	0.5
$\langle E_\gamma \rangle$ (GeV)					
34	3	11	10	12	5
56	5	12	9	10	4
77	5	13	8	9	3
106	5	13	7	8	3
140	5	14	7	8	3

Figure 10 presents the basic ψ-production results, in the form of cross sections for the equivalent flux[17] of transversely polarized virtual photons. Since the Q^2-averaged best-fit physical value of σ_L/σ_T in these data is zero, we neglect any longitudinal cross-section at the present statistical level. In order to suppress contamination from $\psi' \to \psi$+hadrons and from other inelastic processes, the energy deposit in the calorimeter is required not to exceed an amount consistent with elastic ψ-production. The E_γ-dependence in Fig. 10(a) is obtained assuming that the photon cross section has the Q^2-dependence given by the solid line in Fig. 10(b), and vice versa. In order to make comparison with SLAC data[13] accumulated mainly at $t \approx 0$, we express the observed cross-section for ψ photoproduction in terms of $d\sigma/dt(t=0)$. This is done by assuming in the Monte Carlo that $d\sigma/dt(t=0)$ has the value indicated by the solid line in Fig. 10(a). The cross-section over all t is obtained using Eq. (1). The quoted values of $d\sigma/dt(t=0)$ are equal to the solid line multiplied by the ratio of subtracted real data to Monte Carlo data within each E_γ bin. This procedure corrects precisely for acceptance, nuclear coherence, shadowing, and $|t|_{min}$ effects. It should be remembered, however, that the measured quantity is the cross section rather than its intercept at t=0; the intercept could be affected by variations of the t slope over the energy range. Significant variations of this sort are not observed when the SLAC[13] and Fermilab[11] ψ-photoproduction data are compared.

Over the range of $\langle E_\gamma \rangle$ (34 to 140 GeV) the ψ-production cross-section is observed in Fig. 10(a) to rise by a factor close to 2. While a QCD calculation[18] using photon-gluon-fusion also predicts a significant rise in this energy region (hatched band), that rise is seen upon close examination to be significantly larger than can be accomodated by these data. Both the calculation and the data evaluate σ rather than $d\sigma/dt(t=0)$; each in the same way has been con-

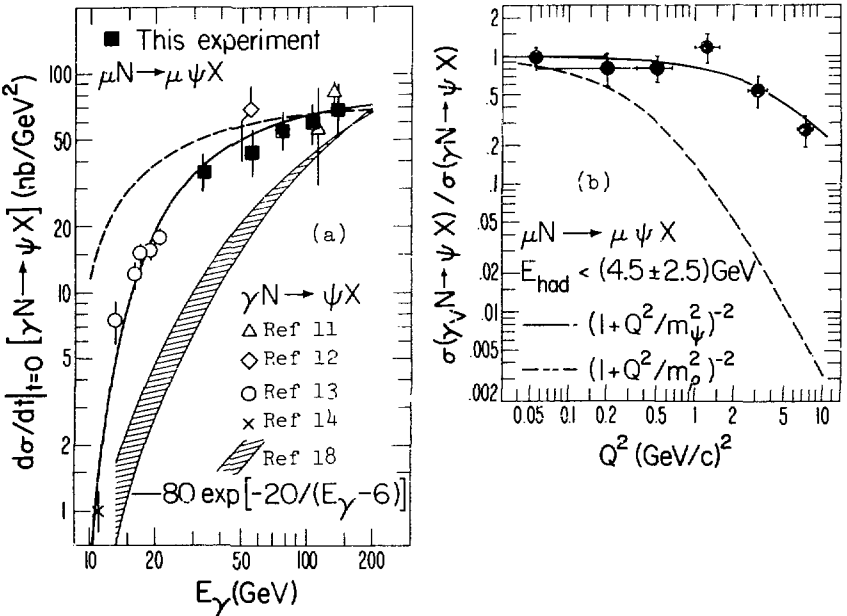

Fig. 10. Cross sections for ψ production by the equivalent flux of virtual photons. (a) E_γ-dependence at t=0. The muoproduction points have an overall ±30% normalization uncertainty (not shown). (b) Q^2-dependence, normalized to 1 at the lowest Q^2 point. Horizontal error flags show typical Q^2 resolution.

verted to $d\sigma/dt(t=0)$ for display in Fig. 10(a). Within vector-meson dominance (VMD), the ratio of the solid line to the broken line ($p^{\psi}_{c.m.}/p^{\gamma}_{c.m.}$) gives the energy-dependence of the square of the ψ-nucleon total cross section. Taking together all data in Fig. 10(a), the threshold behavior of ψ photoproduction now has been measured more precisely than, for example, that of ϕ photoproduction.

Figure 10(b) establishes the shallow Q^2-dependence of ψ photoproduction. The data have been normalized to the lowest-Q^2 point as an approximation to $Q^2=0$. The result fits a propagator-dependence $(1+Q^2/M^2)^{-2}$ with M=2.7±0.5 GeV. Within VMD, consistency of M with the ψ mass implies that no additional Q^2-dependence is needed to parameterize the γ-ψ coupling. The kinematics of photon-gluon-fusion also produce a Q^2-dependence similar to that observed, although the QCD calculations[18] are not presented in a form easy to compare with Fig. 10(b). If these calculations can possess fundamental validity, the broad range of parameters measurable in ψ production by muons can provide many of the crucial tests.

I am pleased to acknowledge the considerable efforts made by Fermilab in behalf of this experiment, and in particular the cooperation of its Neutrino Department. I am very grateful for the hard work of my experimental colleagues and the collaborating support groups. In particular, Mr. T. Markiewicz contributed directly and substantially to the analysis of ψ production. I wish especially to acknowledge the basic contributions made by Mr. J. Caron to the analysis of multimuon final states in two experiments, both as a programmer and as a physicist. This work was supported by the High Energy Physics Division of the U.S. Department of Energy under contract Nos. W-7405-Eng-48, EY-76-C-02-3072, and EY-76-C-02-3000.

1. R. Cester, C.M. Hoffman, M. Strovink, and F.C. Shoemaker, Fermilab Proposal 203 (1973, unpublished).
2. Reviewed by S.C.C. Ting, Rev. Mod. Phys. 49, 235 (1977); B. Richter, Rev. Mod. Phys. 49, 251 (1977).
3. A.R. Clark, E.S. Grove, L.T. Kerth, S.C. Loken, M. Strovink, W.A. Wenzel, R. Cester, F.C. Shoemaker, P. Surko, M.S. Witherell, and R.P. Johnson, Fermilab Proposal 391 (1975, unpublished).
4. Y. Watanabe, L.N. Hand, S. Herb, A. Russell, C. Chang, K.W. Chen, D.J. Fox, A. Kotlewski, P.F. Kunz, S.C. Loken, M. Strovink, and W. Vernon, Phys. Rev. Lett. 35, 898 (1975); C. Chang, K.W. Chen, D.J. Fox, A. Kotlewski, P.F. Kunz, L.N. Hand, S. Herb, A. Russell, Y. Watanabe, S.C. Loken, M. Strovink, and W. Vernon, Phys. Rev. Lett. 35, 901 (1975).
5. G. Gollin, M.V. Isaila, F.C. Shoemaker, and P. Surko, IEEE Trans. Nuc. Sci. NS-26, 59 (1979).
6. T. Hansl et al., Phys. Lett. 77B, 114 (1978).
7. M. Holder et al., Phys. Lett. 73B, 105 (1978).
8. P.J. Loveless et al., Phys. Lett. 78B, 505 (1978).
9. A. Benvenuti et al., Phys. Rev. Lett. 42, 1024 (1979).
10. V. Barger, W.Y. Keung, and R.J.N. Phillips, Univ. of Wisconsin preprint COO-881-83 (1979).
11. B. Knapp et al., Phys. Rev. Lett. 34, 1040 (1975); W.Y. Lee, in Proc. Int. Symp. on Lepton and Photon Interactions at High Energies (DESY, Hamburg, 1977); M. Binkley, private communication.
12. T. Nash et al., Phys. Rev. Lett. 36, 1233 (1976).
13. U. Camerini et al., Phys. Rev. Lett. 35, 483 (1975).
14. B. Gittelman et al., Phys. Rev. Lett. 36, 1616 (1975).
15. See, for example, A. Silverman, in Proc. Int. Symp. on Electron and Photon Interactions at High Energies (Daresebury, 1969), Table 2.
16. W.R. Ditzler et al., Phys. Lett. 57B, 201 (1975).
17. L.N. Hand, Phys. Rev. 129, 1834 (1963).
18. M. Glück and E. Reya, Phys. Lett. 79B, 453 (1978); M. Glück and E. Reya, DESY preprint 79/05 (1979). In Fig. 10(a) we have multiplied their result for σ by 2.4 to obtain $d\sigma/dt(t=0)$.